A Low-power and High-gain Converter for Driving Dielectric Elastomer Actuators

Chen Chen[1], *Student Member, IEEE,* Yichao Tang[1], *Student Member, IEEE,*
Alireza Khaligh[1,2], *Senior Member, IEEE,* and Robert W. Newcomb[1], *Life Fellow*, *IEEE*

Power Electronics, Energy Harvesting and Renewable Energies Laboratory
[1]Electrical and Computer Engineering Department; [2]Institute for Systems Research
University of Maryland, College Park, MD 20742
Email: khaligh@ece.umd.edu; URL: www.ece.umd.edu/~khaligh

***Abstract*- Dielectric elastomers are being used as actuators to convert electrical energy to mechanical deformation in a wide variety of potential microrobotic applications. Majority of these actuators are being excited using external bulky power supplies, which limit the functionality of the actuator. One of the major challenges towards enabling operation of these applications without an external power source is development of lightweight and high power density power electronic interfaces (PEI) with very high step-up gains. This manuscript proposes a special circuit topology to drive dielectric elastomers. The experimental validation has been carried out to verify ability of the circuit to drive a 600V dielectric elastomer at 4Hz for microrobotic applications.**

***Keywords:* dielectric elastomers, lightweight, high power density, power electronic interfaces, high step-up gains, microrobotic applications**

I. INTRODUCTION

Robotic and micro-robotic insects are new family of biomimetic robots, which are inspired from biological insects. The main focus of such robots is to achieve very small size, high maneuverability, and remote controllability [1],[2]. In comparison to other actuators, the dielectric elastomer actuators have advantages, such as higher actuation strain, elastic energy density, and coupling efficiency [3]. The operation principle of a dielectric elastomer actuator (DEA) is illustrated in Fig. 1. The electrostatic force, generated between two electrodes as a result of applying a high DC drive voltage (500V~1kV) across two surfaces, squeezes and extends the elastomer film [4],[5]. Researchers have made advancements in biomimetic robots, using dielectric elastomers as motion actuators [7],[8]. Dielectric elastomers have also been used as prime bistable actuators for binary robotics [9].

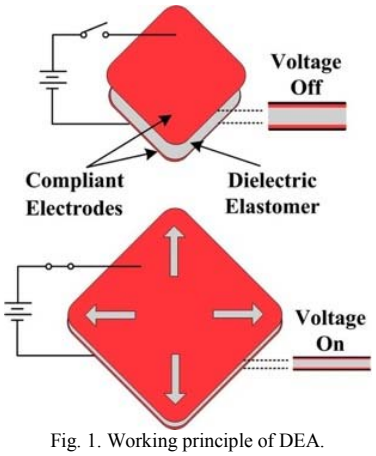

Fig. 1. Working principle of DEA.

An available configuration of DEA is a "bimorph", which contains two compliant electrodes, one as the top surface and the second one as the bottom surface, with a compliant elastomer film inserted in the middle. An efficient drive method is called "Simultaneous Drive" [1]. The scheme of simultaneous drive is shown in Fig. 2. A DC bias drive stage is connected to the two compliant electrodes, while a sinusoidal unipolar drive stage is applied to drive the central compliant elastomer film.

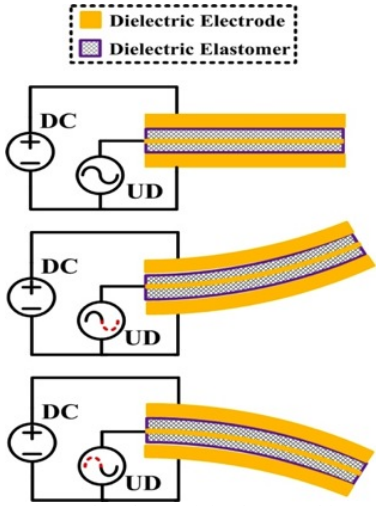

Fig. 2. The scheme of simultaneous drive.

There are two main challenges in driving aforementioned DEA: (a) a high excitation voltage is required and (b) due to stringent size and mass requirements of microrobotic applications, the power electronic interface (PEI) should have high power density and high energy efficiency. Usually, these actuators are being driven by low input voltage sources such as conventional chemical batteries, super-capacitors [13], fuel cells [14], and solar cells [15]. Generally, the output voltage of these energy sources is less than 5V, while the range of required driving voltage for DEA is as high as 1kV [16-18]. Hence, PEI converters with high step-up conversion ratios are necessary.

The overall purpose of this paper is to present a driver topology, which can overcome the abovementioned challenges of high step-up conversion ratio, high energy efficiency, low mass, ultra-compact size and high power density for microrobotic applications. This manuscript is organized as follows. Section II presents a cascade tapped-inductor (TPI) boost converter integrated with a switching amplifier drive stage, the basic operaion theroy,

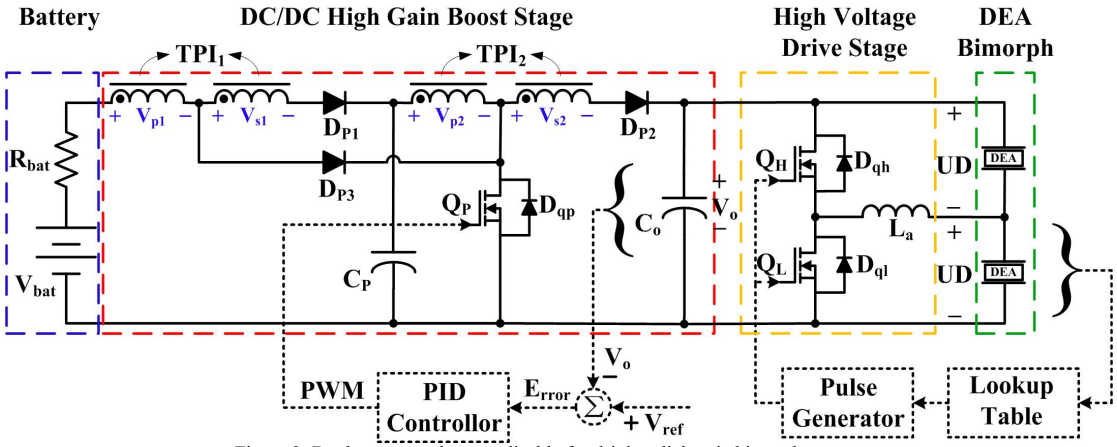

Figure 3: Dual-stage topology applicable for driving dielectric bimorph actuators.

steady-state behavior analysis, control architecture and idealized switching waveforms for illustrated topology. Furthermore, physical implementation of the driving topology, including lightweight package components, converter unit assembly with low computational requirements, and design of custom Printed-Circuit-Board (PCB) at ultra light-scale to meet the strict requirements of microrobotic applications are described in Section III. Finally Section IV presents the conclusions and future research direction.

II. PROPOSED POWER CIRCUIT

Due to the high voltage gain requirement of DEAs, a boost-type cascaded topology is necessary. A cascade TPI boost converter integrated with a switching amplifier drive stage, as depicted in Fig. 3, is chosen. Two cascade TPIs with one MOSFET are employed to obtain the desired high gain with lower duty cycle in comparison to the topologies proposed in the literature [6,10-12]. The switching amplifier drive stage is capable of effectively generating required driving signal and efficiently recovering unused energy.

The two operation modes of the cascade TPI boost circuit are demonstrated in Fig. 4. The TPIs are charged by the input source through the primary windings in Mode I, when the switch Q_P is turned on. As soon as the switch is turned off in Mode II, the diodes start to conduct and the energy is released through the secondary windings of TPIs.

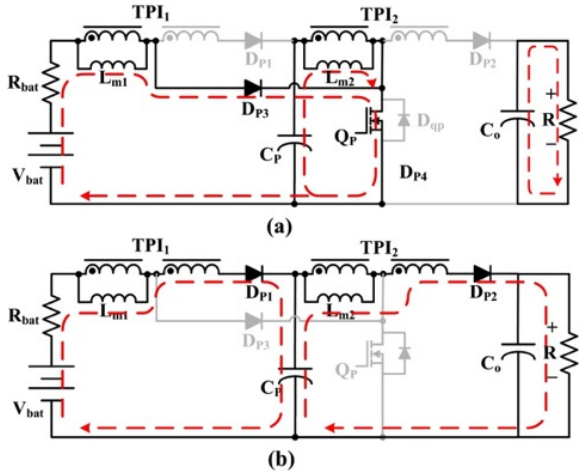

Fig. 4. (a) Mode I: switch is on. (b) Mode II: switch is off.

L_{m1} and L_{m2} are the magnetizing inductances of TPI_1 and TPI_2, respectively.

According to the literature [10], the relationship between I_{p1on} and I_{p1off} is as following:

$$I_{p1on} = (N+1) \cdot I_{p1off} \tag{2}$$

where, I_{p1on} and I_{p1off} are the input current of TPI_1 when switch Q_P is turned on and off, respectively.

The same relational expression between I_{p2on} and I_{p2off} can be obtianed as:

$$I_{p2on} = (N+1) \cdot I_{p2off} \tag{3}$$

where, I_{p2on} and I_{p2off} are the input current of TPI_2 when switch Q_P is turned on and off, respectively.

In accordance with above equations, two complete switching cycle waveforms of DC/DC high-gain boost stage are shown in Fig. 5.

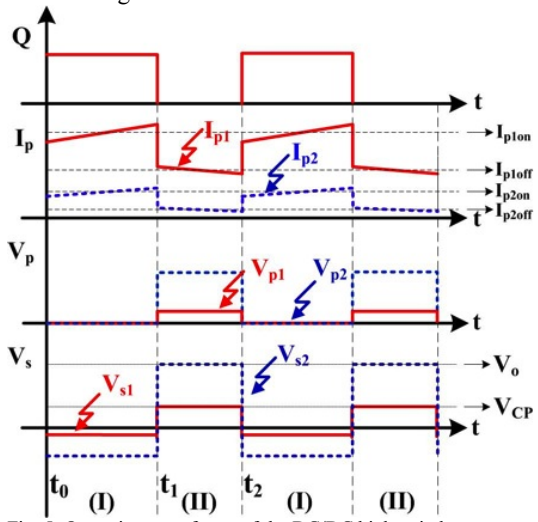

Fig. 5. Operation waveforms of the DC/DC high-gain boost stage.

The proposed DC/DC high-gain boost stage is operated in steady-state Continuous Conduction Mode (CCM). Due to the voltage-second balance principle [19], the average stored/discharging magnetic flux over each switching cycle is zero, as long as the magnetic core does not saturate. The equations for each sub-circuit are as following:

During switching interval (t_0<t<t_1):

$$\frac{\partial i_{p1on}}{\partial t}=\frac{V_{bat}}{L_{m1}} \tag{4}$$

$$\frac{\partial v_{cp}}{\partial t}=-\frac{I_{p2on}}{C_p} \tag{5}$$

During switching interval ($t_1<t<t_2$),

$$\frac{\partial i_{p1off}}{\partial t}=\frac{V_{bat}-V_{cp}}{L_{eq1}} \tag{6}$$

$$\frac{\partial v_o}{\partial t}=\frac{I_{p1off}}{C_p}-\frac{I_{p2on}}{C_p} \tag{7}$$

L_{eq1} is the equivalent coupled inductance of TPI_1, when the magnetic element is discharged.

The same principle is also valid for the TPI_2 boost stage. When the switch is on,

$$\frac{\partial i_{p2on}}{\partial t}=\frac{V_{cp}}{L_{m2}} \tag{8}$$

$$\frac{\partial v_o}{\partial t}=-\frac{V_o}{RC_o} \tag{9}$$

As soon as the switch is turned off and the diodes are on,

$$\frac{\partial i_{p2off}}{\partial t}=\frac{V_{cp}-V_o}{L_{eq2}} \tag{10}$$

$$\frac{\partial v_o}{\partial t}=\frac{I_{p2off}}{C_o}-\frac{V_o}{RC_o} \tag{11}$$

L_{eq2} is the equivalent coupled inductance of TPI_2 during the discharging cycle of the magnetic element.

From the derivation of above equations, the average model of the converter can be obtained as:

$$\dot{x}=\bar{A}\cdot x+\bar{B}\cdot u \tag{12}$$

where, $x=[I_{p1on},I_{p2on},V_{cp},V_o]\in R^4$ is the corresponding state vector of the average model, $u\in R$ is the input voltage, $\bar{A}$ is the system matrix $R^{4\times4}$, $\bar{B}$ is the input vector R^4.

For the the proposed DC/DC high-gain boost stage illusreated in Fig. 3, the corresponding low-frequency model can be expressed as:

$$\begin{bmatrix} I_{p1on} \\ I_{p2on} \\ V_{cp} \\ V_o \end{bmatrix}=\begin{bmatrix} 0 & 0 & \frac{1-D}{(N+1)L_{m2}} & 0 \\ 0 & 0 & \frac{ND+1}{(N+1)L_{m2}} & -\frac{1-D}{(N+1)L_{m2}} \\ \frac{1-D}{(N+1)C_p} & -\frac{1}{C_p} & 0 & 0 \\ 0 & \frac{1-D}{(N+1)C_o} & 0 & -\frac{1}{RC_o} \end{bmatrix}\cdot\begin{bmatrix} I_{p1on} \\ I_{p2on} \\ V_{cp} \\ V_o \end{bmatrix}+\begin{bmatrix} \frac{ND+1}{(N+1)L_{m1}} \\ 0 \\ 0 \\ 0 \end{bmatrix}\cdot V_{bat} \tag{13}$$

In steady state, the step-up gain of the proposed DC/DC high-gain boost stage operating in CCM can be written as

$$G=\frac{V_o}{V_{bat}}=(\frac{ND+1}{1-D})^2 \tag{14}$$

where, $N_1=N_2=N$ is the turns ratio of two TPIs and D is the duty cycle of PWM drive signal for MOSFET Q_P. The voltage gain is relatively higher in comparison to those of the conventional boost converter and single-stage TPI boost converter [10]. The gain-to-control curves of three boost circuits are demonstrated comparatively in Fig. 6, for N=7.

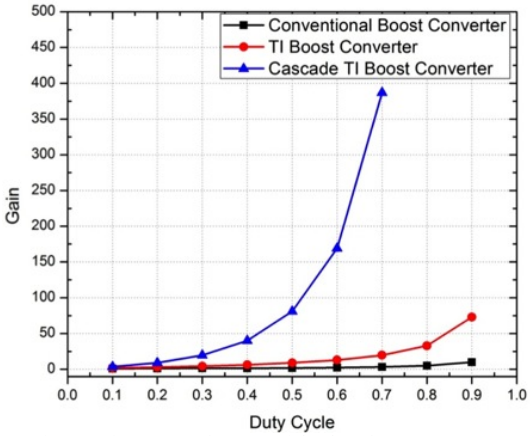

Fig. 6. Gain-to-control curves of the three boost converters.

In order to obtain the transfer function of the proposed DC/DC high-gain boost stage, the method of average state variables decribed in [19] is used. The small signal voltage-to-control transfer function $G_{vd}(s)$ adopted in Proportional Integral Derivative (PID) controller is given in Eq. (15), as:

$$\frac{\tilde{v}_o}{\tilde{d}}=\frac{-s[\frac{I_{p2on}}{(N+1)C_o}]+\frac{1-D}{(N+1)C_o}(\frac{V_{cp}}{L_{m2}}+\frac{V_o-V_{cp}}{(N+1)L_{m2}})}{s^2+s(\frac{1}{RC_o})+\frac{(1-D)^2}{(N+1)C_oL_{m2}}} \tag{15}$$

The high voltage drive stage, demonstrated in Fig. 3, utilizes an LC resonant circuit to create unipolar actuation. The bidirectional circuit is capable of recovering energy through energy transmitting between the loads in each cycle. By using an inductor with low energy loss and two dielectric elastomer actuators, which inherently behave capacitive, a unipolar output actuation signal can be generated.

The four switching modes are presented in Fig. 7. In Mode (a), switch (Q_H) is open and Q_L is closed, the inductor current (I_{La}) increases and energy is transferred to node V_a. In Mode (b), both Q_H and Q_L are turned off, the inductor current (I_{La}) decreases via the freewheel diode (D_{ql}). As soon as the switch Q_L is turned on, the circuit starts to operate in Mode (c). The inductor current (I_{La}) rises in opposite direction and begin to discharge energy through node V_a. In Mode (d), both Q_H and Q_L are turned off, the inductor current (I_{La}) decreases and flows through the freewheel diode D_{qh}.

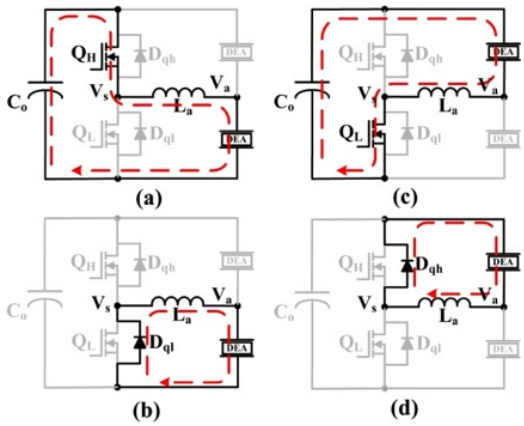

Fig. 7. Four switching modes of high voltage drive stage.

One conventional approach to generate a sinusoidal actuation signal is to use Sinusoidal PWM (SPWM), which strongly depends on LC resonance. Dielectric elastomer actuators are preferred to be driven with a 2~5 Hz low frequency voltage in order to obtain adequate response time. An inductor and two capacitors with footprint of at least 10 mm^2 would be required, in the case of SPWM technology. In order to reduce the size of the passive components (L and C), it is preferred to utilize an Analog to Digital Converter (ADC), a lookup table and a pulse generator. After sampling by the ADC, the output actuation signal is compared with the desired waveform lookup table to generate a real time pulse signal [1]. The voltage and current waveforms during each half cycle are illustrated in Fig. 8.

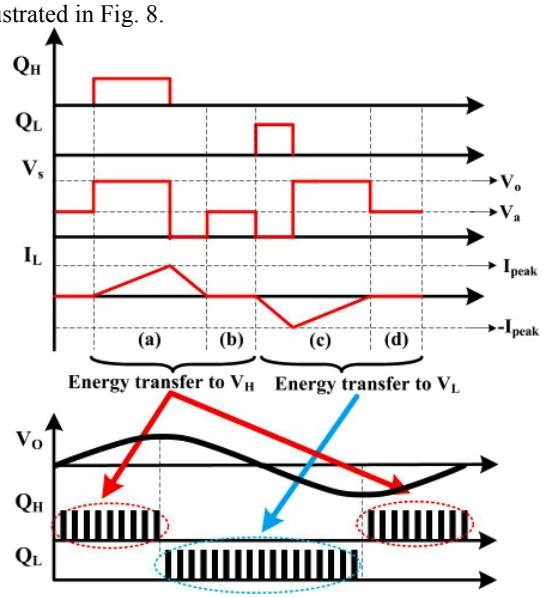

Fig. 8. The inductor current, output voltage, and switching pulse waveforms during each half cycle.

III. FABRICATION SPECIFICATIONS

With respect to stringent size requirement in microrobotic application, it is desirable to use chip-scale package instead of through-hole packaged components [2]. Surface mount components are robust and convinient to be wire-bonded directly on top of the circuit substrate. In consideration of high performance and compact package, components are seriously selected for implementation. The circuit, as depicted in Fig. 3, is fabricated with conventional discrete components soldiered on a Printed Circuit Broad (PCB).

The power stage of the cascade TPI boost converter consists of a power MOSFET switch, three diodes, two coupled inductors and two filter capacitors, which are required to select carefully in order to handle the voltage and current without any breakdown or failure. The expected input voltage range is 3V-5V with a maximum peak current of 200mA. The output voltage is clamped at 600V with the maximum current not exceeding 10mA.

A low profile shielded coupled inductor from Coilcraft, with an excellent coupling coefficient (k = 0.95), is made of ferrite material and weighs as low as 0.3g [20]. N-channel enhancement mode VISHAY MOSFET (IRFBG30) with TO-220 package is selected due to its high-voltage capacity. Three rectifier diodes with low-voltage drops are utilized, which can be replaced with surface-mount package in order to further reduce the PCB dimension. Polarized capacitors with surface mount package are capable of diminishing the voltage ripple on the actuation outputs.

In the case of the drive stage, two N-channel enhancement mode Fairchild Semiconductor MOSFETs (FQD2N100TF) are adopted, which are capable of handling high voltages up to 1kV. A low profile shielded surface mount inductor, with good EMI characteristics, guarantees high quality of output actuation signal. The Q-factor of the designed passive inductor is demanded to be large enough in order to reduce power loss.

The circuit illustrated in Fig. 3 is fabricated with surface mount components soldiered on a PCB. The key specifications of the converter are listed in Table I.

TABLE I
COMPONENT SPECIFICATIONS

	Weight (mg)	Size (mm)	Chip Number
Coupled Inductor	300	6.2×6.8	CJ5143-AL
Switch (Power Stage)	380	14×10	IRFBG30
Rectifier Diode	8	2.8×2.1	1N4007
Capacitor (Power Stage)	6	4.5×3.2	1μF/1kV
Switch (Drive Stage)	380	14×10	FQD2N100TF
Inductor (Drive Stage)	1.2	1.0×0.5	15μH

IV. EXPERIMENTAL RESULTS

A 3.7 V lithium battery performs as the input source of the boost converter. The output dc voltage (V_o) is being regulated at 600V. During the pre-test, the dual-stage converter is capable of driving 1.5MΩ pseudo capacitive loads, which represent dielectric elastomer bimorphs, at 0.5W power.

Fig. 10 demonstrates the efficiency of the DC/DC stage of the proposed converter with respect to various output voltages and output powers. The output voltage of the DC-DC conversion stage vary from 50V to 600V with 50V intervals. The peak efficiency occurs at 300V drive voltage and 0.1W output power.

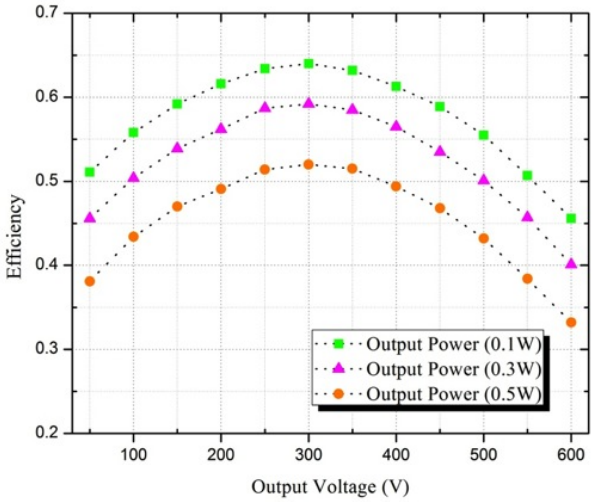

Fig. 10. Efficiency vs. output voltage of DC/DC high-gain boost stage for three dfferent levels of output power.

Fig. 11 shows various driving signals, which are generated from the power converter with a Tadiran 3.7 V

non-rechargeable lithium battery TLH-2450 as the input. Finally, the proposed circuit is driving a bidirectional dielectric elastomer actuator [21], with 600V bias voltage regulated at the output of DC-DC conversion stage. The two drive signals are resonant at 4Hz with 180° phase delay. This circuit is able to generate various types of signals, including square (Fig. 11a), triangle (Fig. 11b), and sinusoidal (Fig. 11c) actuation signals.

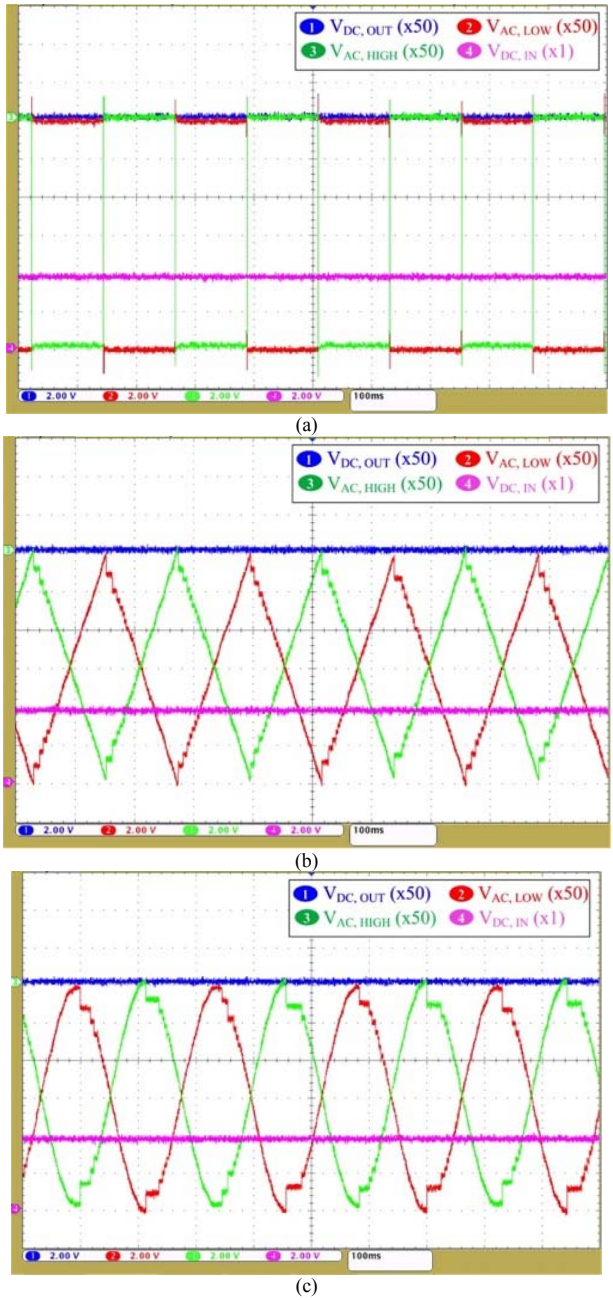

(a)

(b)

(c)

Fig. 11. Experiment result demonstrating the excitation output voltages (VAC,LOW and VAC,HIGH) with (a) square actuation, (b) triangle actuation, and (c) sinusoidal actuation. Note: Tektronix high voltage probe-TPP0850 with 50x attenuation is used to detect 600V voltage.

The overall characteristics of the power electronic circuit is outlined in Table II. In its current design the circuit demonstrate 0.28 kW/kg power density at 500mW output power. The overall maximum efficiecny of the converter considering both DC/DC and drive stages is 35%. The circuit will be significantly improved in terms of size, mass, power density and efficiency. Flexible PCB technology and bare-die components will be introduced so as to achieve the highly integration demand.

Table II
CHARACTERISTICS of POWER CONVERTER

Converter Mass (excluding the PCB and controller weight)	1.78 g
Maximum Power Density	0.28 kW/kg
Maximum Efficiency	35 %

V. CONCLUSIONS AND FUTURE WORK

This paper proposes a specified power electronic interface to drive high-voltage bimorph DEAs. A low-power high-gain DC/DC boost converter and a DC/AC unipolar drive stage, along with their operation modes, are presented in detail. Furthermore, a particular driving approach, instead of conventional SPWM, is introduced to drive bimorph DEA at low frequency. Circuit components prefer to use surface mount package instead of through-hole package to eliminate a large portion of interface size and weight for the sake of on-board capability. The future work is aiming to explore fabrication approaches and high-gain circuit topologies that can further minimize the PCB size and weight for autonomous micro-robotic applications.

ACKNOWLEDGMENT

This work has been sponsored partly by the Minta Martin Aeronautical Research Fund, which is gratefully acknowledged.

REFERENCES

[1] M. Karpelson, G. Y. Wei and R. J. Wood, "Driving high voltage piezoelectric actuators in microroboticapplications," Sensors and Actuators a-Physical, vol. 176, pp. 78-89, Apr. 2012.

[2] M. Karpelson, J. P. Whitney and G.-Y. Wei, "Design and Fabrication of Ultralight High-Voltage Power Circuits for Flapping-Wing Robotic Insects," in Proc. Applied Power Electronics Conference and Exposition (APEC), Fort Worth,Texas, Marc. 2011.

[3] P. Brochu and Q. B. Pei, "Advances in Dielectric Elastomers for Actuators and Artificial Muscles," Macromolecular Rapid Communications, vol. 31, no.1, pp. 10-36,Jan 4 2010

[4] P. Lotz, M. Matysek and H. F. Schlaak, "Fabrication and Application of Miniaturized Dielectric Elastomer Stack Actuators," IEEE Transactions on Mechatronics, vol. 16, no. 1, pp. 58-66, Febr. 2011.

[5] S. Rosset, M. Niklaus and P. Dubois,"Large-Stroke Dielectric Elastomer Actuators With Ion-Implanted Electrodes," Journal of Microelectromechanical Systems, vol. 18, no. 6, pp. 1300-1308, Dece. 2009.

[6] F. L. Luo and H. Ye, "Positive output cascade boost converters," IEEE Proceedings-Electric Power Applications, vol. 151, pp. 590-606, no. 5, Sept. 2004.

[7] F. Carpi, P. Chiarelli and A. Mazzoldi, "Electromechanical characterisation of dielectric elastomer planar actuators: comparative evaluation of different electrode materials and different counterloads," Sensors and Actuators a-Physical, vol. 107, pp. 85-95, Octo. 2003.

[8] R. Pelrine, R. Kornbluh and Q. Pei,"Dielectric elastomer artificial muscle actuators: Toward biomimetic motion," SPIE Smart Structures and Materials, Electroactive Polymer Actuators and Devices, vol. 4695, pp. 126–137, 2002.

[9] P. Chouinard and J. Plante, "Bistable Antagonistic Dielectric Elastomer Actuators for Binary Robotics and Mechatronics," IEEE/ASME Transactions on Mechatronics, vol. PP, no. 99, pp. 1-9, May. 2011.

[10] N. Vazquez, L. Estrada and C. Hernandez, "The tappedinductor boost converter, " in Proc. IEEE Int. Symposium on Industrial Electronics, Vigo, Spain, June. 2007.

[11] F. L. Luo and H. Ye, "Positive output cascade boost converters," IEE Proceedings-Electric Power Applications, vol. 151, no. 5, pp. 590-606, Sept. 2004.
[12] W. C. Liao, T. J. Liang and H. H. Liang, "Study and Implementation of a Novel Bidirectional DC-DC Converter with High Conversion Ratio," in Proc. IEEE conf. on Energy Conversion Congress and Exposition (ECCE), Phoenix, AZ, Sept. 2011.
[13] A. Burke, "Ultracapacitor technologies and application in hybrid and electric vehicles," International Journal of Energy Research, vol. 34, Feb 2010, pp. 133-151.
[14] A. Wilhelm, B. W. Surgenor, and J. G. Pharoah, "Evaluation of a micro fuel cell as applied to a mobile robot," in IEEE Int. Conf. on Mechatronics and Automation, 2005, pp. 32–36.
[15] C. L. Bellew, S. Hollar, and K. S. J. Pister, "An SOI process for fabrication of solar cells, transistors and electrostatic actuators," in IEEE Int. Solid-State Sensors and Actuators Conf., June 2003, pp. 1075–1078.
[16] P. Lotz, M. Matysek and H. F. Schlaak, "Fabrication and Application of Miniaturized Dielectric Elastomer Stack Actuators," IEEE Transactions on Mechatronics, vol. 16, Feb 2011, pp. 58-66.
[17] S. Rosset, M. Niklaus and P. Dubois,"Large-Stroke Dielectric Elastomer Actuators With Ion-Implanted Electrodes," Journal of Microelectromechanical Systems, vol. 18, Dec 2009, pp. 1300-1308.
[18] F. L. Luo and H. Ye, "Positive output cascade boost converters," IEEE Proceedings-Electric Power Applications, vol. 151, Sep 2004, pp. 590-606.
[19] R. W. Erickson, "DC-DC power converters", Wiley Encyclopedia of Electrical and Electronics Engineering, 1988: Wiley.
[20] "CJ5143-AL Flyback Transformer for ON Semiconductor NCP5080 Photoflash Capacitor Charger," Product Data Sheet, Coilcraft Corp., 2009.
[21] A. P. Gerratt, B. Balakrisnan, and S. Bergbreiter, "Batch microfabricated bidirectional dielectric elastomer actuators," in Transducers, Beijing, June 5-9, 2011.